Coulomb stresses imparted by the 25 March 2007 $M_{\rm w}$=6.6 Noto-Hanto, Japan, earthquake explain its 'butterfly' distribution of aftershocks and suggest a heightened seismic hazard

Shinji Toda

Active Fault Research Center, Geological Survey of Japan, National Institute of Advanced Industrial Science and Technology (AIST), site 7, 1-1-1 Higashi Tsukuba, Ibaraki 305-8567, Japan

The well-recorded aftershocks and well-determined source model of the Noto Hanto earthquake provide an excellent opportunity to examine earthquake triggering associated with a blind thrust event. The aftershock zone rapidly expanded into a 'butterfly pattern' predicted by static Coulomb stress transfer associated with thrust faulting. We found that abundant aftershocks occurred where the static Coulomb stress increased by more than 0.5 bars, while few shocks occurred in the stress shadow calculated to extend northwest and southeast of the Noto Hanto rupture. To explore the three-dimensional distribution of the observed aftershocks and the calculated stress imparted by the mainshock, we further resolved Coulomb stress changes on the nodal planes of all aftershocks for which focal mechanisms are available. About 75% of the possible faults associated with the moderate-sized aftershocks were calculated to have been brought closer to failure by the mainshock, with the correlation best for low apparent fault friction. Our interpretation is that most of the aftershocks struck on the steeply dipping source fault and on a conjugate northwest-dipping reverse fault contiguous with the source fault. Since we found that the Coulomb hypothesis works well for the Noto Hanto sequence, we subsequently computed stress changes on the nearby active faults. Although the calculated stress changes were found to be negligible on the major faults south of the Noto Peninsula, several short active faults near the epicentral area were calculated to have been brought several bars closer to failure. Thus, the probability of strong shaking in and around the epicentral area may still be high due to the transfer of stress to the adjacent faults by a short blind thrust fault.
Key words: 2007 Noto Hanto earthquake, Coulomb stress change, aftershocks, off-fault aftershocks, blind thrust.

1. Introduction

Calculations of static Coulomb stress changes caused by an earthquake have been used to explain the spatial distribution of the subsequent aftershocks (Stein, 1999; Steacy *et al.*, 2005; Freed, 2005 and the references therein). If the hypothesis is sound, then Coulomb stress change provides a tool to forecast the subsequent large earthquake triggering nearby. The correlation between stress change and seismicity rate change has encouraged efforts to develop a practical forecasting model of subsequent seismicity, which has generally been applied to aftershocks (e.g., Toda *et al.*, 2005). One means to test the Coulomb hypothesis is assessing the location of so-called 'off-fault aftershocks'. Lin and Stein (2004) suggest that blind thrusts tend to trigger slip on secondary faults at shallow depth and typically produce broadly distributed aftershocks. Based on diagnostic calculations and examination of a half-dozen California thrust earthquakes, they further argue that short thrust ruptures are particularly efficient at triggering earthquakes of similar size on adjacent thrust faults. Because of Japan's unsurpassed seismic and geodetic networks, as well as the documented coseismic coastal uplift, the 25 March 2007

$M_{\rm j} = 6.9$ ($M_{\rm w} = 6.6$) Noto-Hanto earthquake provides an important opportunity to examine the aftershock triggering process of blind thrust faults.

The Noto-Hanto earthquake struck the northwest coastline of the Noto Peninsula. Similar to the 7 February 1993 $M_{\rm j} = 6.6$ Noto-Hanto-oki earthquake, the Noto Hanto event occurred under NW-SE compressional stress within the shallow crust in the Eurasian plate. On the Noto Peninsula there are many short discrete reverse faults associated with vertical movements, resulting in approximately 10- to 20-km-long small tilted crustal blocks that developed during the late Tertiary period to the Quaternary (Ota, 1975). One of these crustal blocks slipped in the 2007 shock. The focal mechanism of the Noto Hanto earthquake is reverse faulting with a slight right-lateral component, with strike 58°, dip 60°, and rake 117° (USGS, 2007). Seismic inversions (Yagi, 2007; Yamanaka, 2007) also suggest the NE-SW striking and highly SE-dipping blind reverse fault of a magnitude of $M_{\rm w} = 6.7$. Similar to the other cases associated with blind thrust faults (e.g., 2004 $M_{\rm j} = 6.8$ mid-Niigata Prefecture earthquake; Kato *et al.*, 2005), the aftershock sequence of the Noto Hanto earthquake shows significant expansion with time from the source (Fig. 1). In addition, since there are many active faults nearby, it would be necessary to estimate the stresses loaded or removed from the surrounding faults to assess the change in their seismic
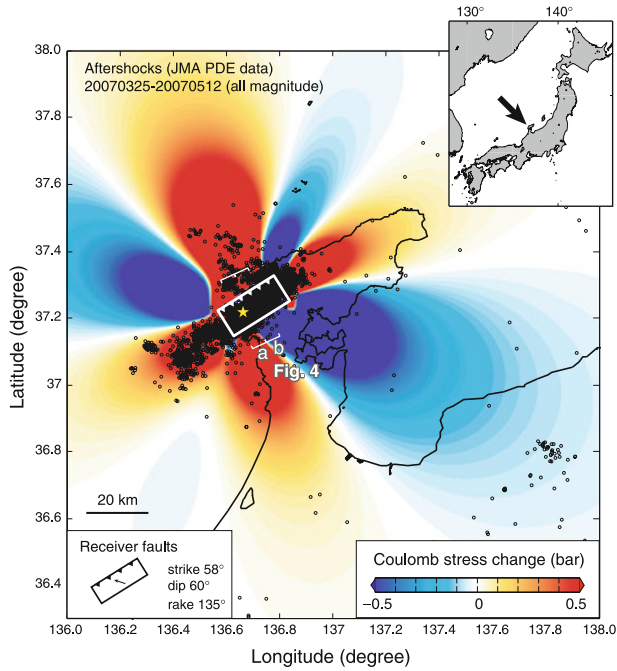
Fig. 1. Aftershocks of the Noto-Hanto earthquake from the Japan Meteo-rological Agency (JMA) catalog superimposed on coseismic Coulomb stress changes on thrust faults at a depth of 10 km, assuming an apparent friction coefficient μ' of 0.4. The white rectangle indicates the map projection of the mainshock source fault, which dips 60° to the southeast. The star is the epicenter determined by the JMA. Two seismic cross-sections across the source fault (a and b) indicated by thin white lines are shown in Fig. 4.

potential. In this paper, we first examine the spatial correlation between aftershocks and Coulomb stress change due to the Noto Hanto earthquake. Using focal mechanism data, we then test whether moderately sized earthquakes were indeed triggered by the mainshock. From this we infer the apparent fault friction and structural control on aftershock occurrence. Finally, we estimate how many stresses are loaded onto major active faults nearby.

2. Static Coulomb Stress Change Throughout the Crust

The static Coulomb stress change caused by a mainshock ΔCFF is calculated by

$$\Delta\text{CFF} = \Delta\tau + \mu(\Delta\sigma + \Delta p) \quad (1)$$

where $\Delta\tau$ is the shear stress change on a given fault plane (positive in the direction of a long-term fault slip), $\Delta\sigma$ is the fault-normal stress change (positive for unclamping), μ is the coefficient of friction, and Δp is the pore pressure change within the fault. This equation can be reformulated as,

$$\Delta\text{CFF} = \Delta\tau + \mu'\Delta\sigma \quad (2)$$

where μ' is the apparent friction, which includes the effect of the pore pressure change associated with the normal stress change (Cocco and Rice, 2003). We compute the Coulomb stress change in an elastic half-space (Okada, 1992) under the assumption that a shear modulus of 3.2×10^{11} dyn cm^{-2} and a Poisson's ratio of 0.25.

To calculate Coulomb stress change, we use the variable slip model proposed by Horikawa (2008) which is inverted from strong motion data. Horikawa's source fault model is a 22-km-long and 20-km-wide fault plane, striking N58°E and dipping 60°SE, with variable slips along a fixed 135° rake direction (reverse faulting with a slight right-lateral slip component). Although several other variable slip models based on seismic waveform inversion (e.g., Yagi, 2007) have also been proposed, the advantage of using Horikawa's model is the practical location of the fault, which clearly explains the significant coastal uplift across the epicentral region reported by Awata et al. (2007).

In order to examine the relationship between aftershocks and stress changes, we assume that most small to moderate earthquakes dominating in the earthquake catalog are caused by thrust faults under NW-SE compressional regional stress. Although the focal mechanisms of the previous large and moderate size events show some fluctuation in terms of focal mechanisms, we assume here the receiver faults in our study area have a strike of 58°, a dip of 60° to the southeast, and a rake of 135°, which is the same slip direction of the source fault and roughly consistent with most of the strikes of active faults in this area. We have calculated the stress change at a depth of 10 km with an apparent friction $\mu' = 0.4$, which generally minimizes the uncertainty in μ', since it has a possible range of 0–0.8 (King et al., 1994). In Fig. 1, areas of stress increase by more than 0.5 bar (0.05 MPa) show a quadrant 'butterfly pattern' (Stein, 1999), whereas significant stress decreases are evident in the northwest and southeast regions of the source fault. To see the overall spatial relationship between Coulomb stress change and aftershock distribution, we overlay ~50 days of aftershocks onto the Coulomb stress change. Even though the Coulomb hypothesis cannot explain the occurrence along the source fault itself, most of the off-fault aftershocks occurred on all four lobes of Coulomb stress increase. A significant expansion of the off-fault aftershock zone is seen extending southwest, far beyond the western edge of the source fault, up to one-half of the fault length (approx. 30 km). Along the source fault, the smoothed model is probably inadequate to reflect local spikes in stress caused by slip roughness.

3. Coulomb Stress Change on Nodal Planes of Moderately Sized Earthquakes

As suggested by Lin and Stein (2004), stress transfer in a thrust fault system is less well understood that for strike-slip and normal faults because the distribution of stress changes in the thrust faults must be analyzed three dimensionally. Two approaches are generally used to examine the correlation between the Coulomb stress change and aftershock occurrence in thrust fault systems, which exhibit the strong depth dependence of stress changes. One is to study multiple cross sections or depth slices, and the other is to calculate the change in Coulomb stress on the nodal planes of the aftershocks. Here we implement the latter approach. We first collected 50 well-determined focal mechanisms for $M \geq 3.5$ shocks in our study area (Fig. 1), as determined by the F-net broadband network between March 25 and June 11 (NIED, 2007). Most of the mechanisms are NE-trending

Table 1. Selected aftershock focal mechanisms of the Noto Hanto earthqukake and calculated Coulomb stress changes.

ID	origin time (JST) (yr/mo/dy, hr:mn)	moment (N m)*10⁷	M_j	hypocenter		
				longitude (°)	latitude (°)	depth (km)
1	2007/03/25,18:11	6.22	5.3	136.8395	37.3043	8
2	2007/03/26,02:14	7.47	4.2	136.6695	37.1578	8
3	2007/03/26,04:03	2.72	3.5	136.7207	37.3712	5
4	2007/03/26,07:16	4	5.3	136.4893	37.1668	5
5	2007/03/26,14:42	1.05	3.5	136.5305	37.1712	5
6	2007/03/26,14:46	6.85	4.8	136.5518	37.1653	5
7	2007/03/26,18:35	2.07	3.6	136.5608	37.1630	5
8	2007/03/27,06:48	5.5	3.6	136.5483	37.1802	5
9	2007/03/27,07:16	5.3	4.1	136.5472	37.1143	5
10	2007/03/28,10:51	1.29	4.4	136.6118	37.1757	5
11	2007/03/28,21:16	3.22	3.7	136.5823	37.1903	5
12	2007/03/30,14:04	1.25	3.7	136.5998	37.3042	5
13	2007/04/04,14:12	1.91	3.5	136.5308	37.1615	8
14	2007/04/06,21:42	8.02	4.7	136.4252	37.0955	5
15	2007/04/06,23:55	2.07	4.3	136.4342	37.0922	5
16	2007/04/13,09:02	3.57	3.7	136.5165	37.1687	5
17	2007/04/16,15:29	7.95	4.0	136.5553	37.1802	5
18	2007/04/28,03:15	2.95	3.8	136.6960	37.3300	5
19	2007/05/02,20:44	3.68	4.6	136.7628	37.3307	5
20	2007/05/05,01:11	1.19	4.2	136.4170	37.0737	5
21	2007/05/05,13:26	2.12	3.5	136.4335	37.0755	5
22	2007/05/11,02:12	2.94	4.7	136.3117	37.1185	5
23	2007/05/12,13:42	5.09	3.8	136.5023	37.1683	5
24	2007/05/25,14:08	4.94	3.7	137.6718	36.8723	8

ID	nodal plane1						nodal plane 2					
	strike1 (°)	dip1 (°)	rake1 (°)	ΔCFF (bar)			strike2 (°)	dip2 (°)	rake2 (°)	ΔCFF (bar)		
				$\mu' = 0.0$	$\mu' = 0.4$	$\mu' = 0.8$				$\mu' = 0.0$	$\mu' = 0.4$	$\mu' = 0.8$
1	40	53	101	5.6	6.3	6.9	203	38	76	5.6	2.4	−0.8
2	195	63	102	8.0	9.3	10.5	350	29	68	8.0	11.2	14.4
3	13	53	81	0.9	0.0	−0.9	207	38	102	0.9	0.3	−0.3
4	325	77	17	4.3	2.6	0.9	231	73	166	4.3	3.2	2.2
5	169	58	47	4.3	2.0	−0.2	49	52	137	4.3	4.4	4.4
6	52	71	151	4.9	4.2	3.5	152	63	22	4.9	5.5	6.1
7	24	61	110	5.7	4.6	3.5	166	35	58	5.7	6.1	6.5
8	3	53	122	4.0	2.5	1.0	136	47	54	3.9	5.7	7.4
9	44	63	127	1.3	1.3	1.4	165	45	40	1.2	0.6	0.0
10	60	80	150	−2.0	−20.1	−38.2	156	61	12	−2.1	−27.6	−53.0
11	159	55	45	23.9	19.7	15.5	39	54	135	23.8	24.4	25.0
12	65	85	163	−3.0	1.8	6.5	156	73	5	−2.9	−2.7	−2.5
13	244	88	97	−1.2	−1.9	−2.6	349	7	15	−1.2	−0.9	−0.6
14	16	62	85	0.2	−0.3	−0.7	207	29	99	0.2	0.1	0.1
15	25	56	97	0.4	0.0	−0.3	193	35	80	0.4	0.3	0.3
16	15	60	96	4.9	1.8	−1.3	183	30	80	4.9	3.7	2.5
17	207	89	142	8.3	5.2	2.1	297	52	1	8.3	5.0	1.7
18	32	73	64	−2.4	−1.1	0.3	270	31	145	−2.3	−1.6	−0.8
19	203	71	63	−0.4	−2.9	−5.4	80	33	142	−0.4	−1.9	−3.5
20	33	47	108	0.7	0.5	0.3	188	46	72	0.7	0.3	−0.1
21	12	55	95	1.0	0.5	0.0	183	35	83	1.0	0.7	0.4
22	74	77	146	0.3	0.2	0.2	172	57	16	0.3	0.3	0.3
23	26	46	104	1.7	0.9	0.2	185	46	75	1.7	1.5	1.4
24	352	65	48	−0.1	0.0	0.0	237	47	145	−0.1	0.0	0.0

thrust events mixed with NE-striking right-lateral or NW-striking left-lateral faults. Since the unknown details of the slip distribution and rupture geometry influence the stress changes very close to the source fault, we excluded the 26 shocks closer than approximately 2 km to the main fault rupture (Fig. 2), leaving 24 shocks listed in Table 1 for analysis.

Because we do not know the true rupture plane of each aftershock, we resolved Coulomb stress changes on both nodal planes with three different candidate values of apparent friction: $\mu' = 0.0$, 0.4, and 0.8 (Table 1; Fig. 3). There is no systematic or meaningful grouping (separation) of nodal planes 1 and 2 in Table 1, so the assignment of plane '1' and '2' is random. The case of $\mu' = 0.0$ corresponds to shear stress change which is identical on both nodal planes (there are some slightly different values seen in Table 1 because of the round-off effect in nodal plane information). For $\mu' = 0.0$, 18 out of 24 shocks (75%) are calculated to have occurred on planes on which the shear stress increased. In the case of $\mu' = 0.4$, the mainshock
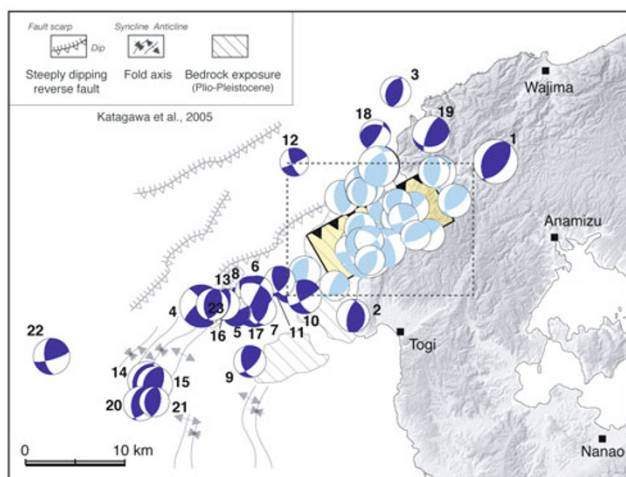
Fig. 2. All well-determined focal mechanisms of $M \geq 3.5$ aftershocks from the F-net broadband network between March 25 and June 11 2007 (NIED, 2007) used for the stress calculations. Underlying graphics are locations of the mainshock source fault (yellow) and active geological structure, as revealed by Katagawa *et al.* (2005). Aftershocks shown as light-blue beach balls located in the area enclosed by dash lines are excluded from stress calculations because they are less than 2 km from the source fault in three dimensions. Numbers beside the blue beach balls are serialized in time and correspond to the ID numbers in Table 1 and Fig. 3.
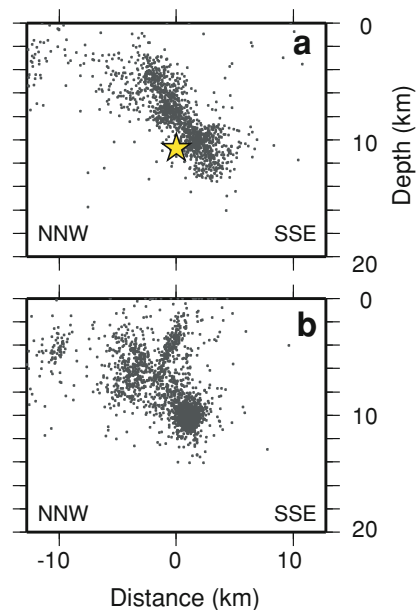

Fig. 4. Cross-sections of the Noto Hanto aftershocks showing the source fault as a highly SSE-dipping blind reverse fault. A steeply dipping conjugate fault is visible in section b. See Fig. 1 for the positions of both cross-sections and information on the earthquake data.

Fig. 3. Coulomb stress changes resolved on aftershock nodal planes under various frictional assumptions. See Table 1 and Fig. 2 for information on each aftershock number aligned along the *x*-axis. Note that about 75% of the aftershocks occurred with positive changes in Coulomb stress.

4. Stress Imparted to Nearby Active Faults

We can easily estimate the amount of stress perturbation on known active faults. If one assumes that the fundamental faulting mechanism is the same for a wide range of magnitudes among triggered shocks and that all shocks exhibit the same range of stress drops, then it is likely that a given increase in Coulomb stress will promote failure regardless of the size of the fault. Here we model the regional active faults discovered and compiled by Ota *et al.* (1976), the Research Group for Active Faults in Japan (1991), and the Headquarters for Earthquake Research Promotion (2005). We then resolve the Coulomb stress change, ΔCFF, onto these surfaces assuming plausible slip directions (rakes) for each. We calculate the ΔCFF at the center of each major active fault that is sufficiently far from the Noto Hanto epicenter to yield a reliable result. For the faults closest to the 2007 Noto Hanto epicenter, we subdivide the faults into several patches in order to calculate the distribution of ΔCFF across the surfaces (Fig. 5). The dips of these thrust faults are assumed to be 55–65°, which is a good compromise among the various independent estimates.

Our model of stress transfer implies that the Noto Hanto earthquake increased the Coulomb stress up to tens of bars toward failure on the closest Sakami fault and the unnamed Quaternary fault extending westward from the source fault, a location where aftershocks are abundant. In contrast, the stress imparted to the NW dipping 'conjugate fault' revealed by the aftershock cross section (Fig. 4) depends on the part and depth of the fault because of its close proximity to the source fault. Low friction is necessary to activate the conjugate fault (inset in Fig. 5). Because of the abundant aftershocks on or near this fault, this fault furnishes perhaps the strongest inference for low friction in the study area. The stress changes resolved on the large active faults

brought 38 of a possible 48 fault planes closer to failure (79%). For the highest apparent friction, $\mu' = 0.8$, the mainshock brought 32 of the 48 planes closer to failure (67%). We therefore concluded that low to moderate friction provides a better fit than high friction. Even though a limited number of focal mechanisms are available and their locations, in particular the hypocentral depth, may not be accurate enough, we suggest that most of the moderate-to large-sized aftershocks may have been triggered by the mainshock stress perturbation.
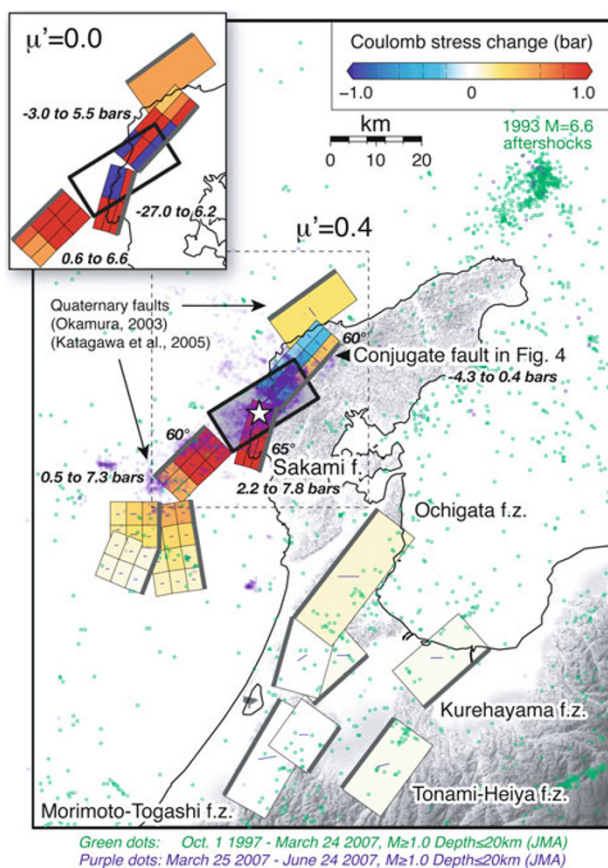
Fig. 5. Coulomb stress changes caused by the Noto Hanto earthquake resolved onto active faults. Locations and slip geometries of the active faults and Quaternary faults are based on Ota *et al.* (1976), Research Group for Active Faults in Japan (1991), Okamura (2003), and Katagawa *et al.* (2005). Thick gray lines indicate the surface projection of each fault; if the gray line is offset from the fault, it is blind. Thin blue lines on each fault give the slip direction (rake) on which stress is resolved. Dips for the active faults are set to 55°, except where otherwise marked. The inset shows the shear stress change ($\mu' = 0.0$) that best explains significant aftershock occurrence along a NW-dipping conjugate fault appearing in seismic cross-section in Fig. 4. Seismicity during the approximately 10-year period immediately preceding the 2007 mainshock and 3-month aftershocks are plotted as green and purple dots respectively.

located in the southern peninsula are calculated to have slightly increased by <0.05 bar (5 kPa), which is almost equivalent to a tidal stress level and, therefore, probably inconsequential. The Coulomb stresses on the other Quaternary faults, which are not assigned as being active in the Holocene period with any degree of confidence, are calculated to have moderately risen by up to 0.3 bar, which may be just above the level of significant seismicity rate change that would be expected (i.e., more than 0.1 bar, Stein, 1999).

5. Discussion and Conclusions

Well-recorded aftershocks of the 2007 Noto Hanto earthquake provide an opportunity to examine the validity of the Coulomb hypothesis in the thrust fault regime. Abundant aftershocks spread widely away from the source fault and showed a 'butterfly pattern', as predicted by the simple Coulomb stress calculation for surrounding thrust faults. Even though we have not performed rigorous statistical tests using all aftershocks, stress changes on available nodal

planes attest that most of the moderate size earthquakes were brought closer to failure by the mainshock.

In the offshore region far west of the epicenter in the Noto Peninsula, Katagawa *et al.* (2005) and Okamura (2003) discovered several blind thrusts that underlie NE-SW- and NS-trending folds as well as clear surface-cutting thrusts (Fig. 2). Focal mechanisms (Fig. 2) and the confined aftershock distribution (Fig. 1) along such fault and fold zones suggest that enhanced Coulomb stress due to the mainshock triggered some slip along the pre-existing fractures, producing small to moderate shocks but not large ones. In other words, numerous repetitions of Noto Hanto-type earthquakes may have developed such geologic structures during the late Quaternary period. Of course it is possible that the correlation between the change in Coulomb stress and the aftershock distribution is fortuitous, with the aftershocks instead governed by pre-existing structural features, as advocated by McCloskey *et al.* (2003) and Imanishi *et al.* (2006).

There may be two explanations for the temporal expansion of the aftershock zone; one is the time-dependent effect of the earthquake nucleation process accelerated by the coseismic stress step, and the other is secondary aftershock triggering. The former concept is often explained by the rate- and state-dependent constitutive formulation of earthquake occurrence given by Dieterich (1994) together with Coulomb stress steps (e.g., Stein *et al.*, 1997). Figure 6 in Dieterich (1994) elucidates how the expansion of aftershock zones is controlled by the stress change normalized by $A\sigma$ (a constitutive parameter $A \times$ the effective normal stress σ). To reproduce the rapid aftershock expansion seen in the Noto Hanto sequence, $A\sigma$ should be quite small. This could be produced by high internal pore pressure, which reduces the effective normal stress σ and is consistent with the relatively low coefficient apparent friction found in this study. In contrast, the role of secondary aftershocks is evident from a number of dense seismic clusters near the moderately sized aftershocks. The epidemic-type aftershock sequence (ETAS) model of Ogata (1988) generally reproduces the entire temporal decay of such secondary aftershocks, although it does not address the spatial distribution, such as the butterfly pattern. Since the ETAS model deals with point processes, multiple stress steps incorporating stress changes due to large aftershocks (e.g., Toda and Stein, 2003) would perform better in capturing the space and time behavior of aftershock sequences.

It is clear from focal mechanism solutions (USGS, 2007; JMA, 2007; NIED, 2007), the geodetic GPS inversion (GSI, 2007), and the aftershock distribution in cross-section that the Noto Hanto source fault dips steeper than 50°. Such a steeply dipping reverse fault originated from a normal fault developed under extensional regime in the Tertiary period (the inversion tectonics in the Noto Peninsula are discussed by Katagawa *et al.*, 2005); such an origin is common to many thrust fault regimes around the globe. As suggested by Sibson (1990), low static friction and/or high differential stress are necessary to activate such a high-angle reverse fault. Our analysis of the Coulomb stress changes on the Conjugate fault (Fig. 3; Table 1) also suggests low to moderate apparent friction rather than high friction. Although

there are several unknown elements associated with the effect of fault-zone fluids and structural heterogeneity in and around the source, the low inferred friction and low inferred value of $A\sigma$ used to account for the rapid aftershock expansion suggest that fluids may have played an important role in the occurrence of earthquakes in and around the hypocentral region.

Coulomb theory is often applied to updating probabilities for large earthquakes nearby (e.g., Parsons *et al.*, 2000). Fortunately, as shown in Fig. 5, the major active faults located in the southern Peninsula are calculated to be largely unaffected by the 2007 Noto Hanto mainshock, and no significant off-fault aftershocks have been associated with them. However, several short active faults in the northern Peninsula are calculated to have been strongly stressed. The Sakami fault, in particular, has been brought more than several bars closer to Coulomb failure by the Noto Hanto earthquake. Even though the Sakami fault may be shorter than 15 km and its paleoseismic history is uncertain, its slip rate (more than 0.4 mm/year vertically; Ota *et al.*, 1976) is high relative to that of the other faults nearby. Since the Sakami fault is very close to the 2007 source fault, it is difficult to identify the particular aftershocks associated with stress increase on the Sakami fault. Nevertheless, we can conclude that the 25 March 2007 event does not reduce the probability for strong shaking on the peninsula. Rather, it may have raised the likelihood of shaking by promoting failure on adjacent thrust faults. Although we can not estimate the time dependency of the stress increase effect on the faults, it is possible that any transient triggering effect on the nucleation process would be diluted rapidly (Dieterich, 1994); however, such a process could last several years to several decades based on the results of previous studies (e.g., Toda and Stein, 2003). Such a hypothesis can be partially validated from the fact that aftershocks associated with the 1993 $M = 6.6$ Noto-Hanto-oki earthquake are still visible (Fig. 5).

References

Awata, Y., S. Toda, H. Kaneda, T. Azuma, H. Horiawa, M. Shishikura, and T. Echigo, Crustal deformation due to the Noto Hanto earthquake in 2007 estimated from the pre-earthquake sea level, *abstract for Japan Geoscience Union Meeting 2007*, http://earth2007.jtbcom.co.jp/session/pdf/Z255/Z255-P022_e.pdf, 2007.

Cocco, M. and J. R. Rice, Pore pressure and poroelasticity effects in Coulomb stress analysis of earthquake interactions, *J. Geophys. Res.*, 107(B2), 2030, doi:10.1029/2002JB001779, 2003.

Dieterich, J., A constitutive law for rate of earthquake production and its application to earthquake clustering, *J. Geophys. Res.*, 99, 2601–2618, 1994.

Freed, A. M., Earthquake triggering by static, dynamic, and postseismic stress transfer, *Annu. Rev. Earth Planet. Sci.*, 33, 335–367, doi: 10.1146/annurev.earth.33.092203.122505, 2005.

Geographical Survey Instutite (GSI), The fault of the Noto Hanto Earthquake in 2007, http://cais.gsi.go.jp/Research/crust/notohanto/fault_model.html, 2007.

Headquarters for Earthquake Research Promotion, Report: 'National Seismic Hazard Maps for Japan (2005)', original version in Japanese, pp. 121, 2005 (translation version released in 2006 is on http://www.jishin.go.jp/main/index-e.html).

Horikawa, H., Characterization of the 2007 Noto Hanto, Japan, earthquake, *Earth Planets Space*, 60, this issue, 1017–1022, 2008.

Imanishi, K., Y. Kuwahara, and Y. Haryu, Off-fault aftershocks of the 2005 west off Fukuoka Prefecture earthquake: Reactivation of a structural boundary?, *Earth Planets Space*, 58, 81–86, 2006.

Japan Meteorological Agency (JMA), CMT solution of the March 25, 2007 Noto Hanto earthquake, http://www.seisvol.kishou.go.jp/eq/mech/cmt/fig/cmt20070325094157.html, 2007.

Katagawa, H., M. Hamada, S. Yoshida, H. Kadosawa, A. Mitsuhashi, Y. Kono, and Y. Kinugasa, *J. Geograph.*, 114, 791–810, 2005 (in Japanese with English abstract).

Kato, A., E. Kurashimo, N. Hirata, S. Sakai, T. Iwasaki, and T. Kanazawa, Imaging the source region of the 2004 mid-Niigata prefecture earthquake and the evolution of a seismogenic thrust-related fold, *Geophys. Res. Lett.*, 32, J07307, doi:10.1029/2005GL022366, 2005.

King, G. C. P., R. S. Stein, and J. Lin, Static stress changes and the triggering of earthquakes, *Bull. Seismol. Soc. Am.*, 84, 935–953, 1994.

Lin, J. and R. S. Stein, Stress triggering in thrust and subduction earthquakes and stress interaction between the southern San Andreas and nearby thrust and strike-slip faults, *J. Geophys. Res.*, 109, B02303, doi:10.1029/2003JB002607, 2004.

McCloskey, J., S. S. Nalbant, S. Steacy, C. Nostro, O. Scotti, and D. Baumont, Structural constraints on the spatial distribution of aftershocks, *Geophys. Res. Lett.*, 30(12), 1610, doi:10.1029/2003GL017225, 2003.

NIED, Earthquake Mechanism Search in F-net Broadband Seismograph Network data, http://www.fnet.bosai.go.jp/freesia/event/search/search.html, 2007.

Ogata, Y., Statistical models for earthquake occurrences and residual analysis for point processes, *J. Am. Stat. Assoc.*, 83, 9–27, 1988.

Okada, Y., Internal deformation due to shear and tensile faults in a half-space, *Bull. Seismol. Soc. Am.*, 82, 1018–1040, 1992.

Okamura, Y., Explanatory notes of geological map west of Noto Peninsula 1:200,000, Marine Geology Map series, 61 (CD), Geological Survey of Japan, AIST, 2003.

Ota, Y., Late Quaternary vertical movement in Japan estimated from deformed shorelines, *The Royal Society of New Zealand Bull.*, 13, 231–239, 1975.

Ota, Y., T. Matsuda, and J. Hirakawa, Active faults in Noto Peninsula, central Japan, *Quat. Res.*, 15, 109–128, 1976 (in Japanese with English abstract).

Parsons, T., S. Toda, R. S. Stein, A. Barka, and J. H. Dieterich, Heightened odds of large earthquakes near Istanbul: An interaction-based probability calculation, *Science*, 288, 661–665, 2000.

Research Group for Active Faults in Japan, *Active Faults in Japan, sheet maps and inventories, rev. ed.*, 437 pp., University of Tokyo Press, Tokyo, 1991.

Sibson, R. H., Rupture nucleation on unfavorably faults, *Bull. Seismol. Soc. Am.*, 80, 1580–1604, 1990.

Steacy, S., J. Gomberg, and M. Cocco, Introduction to special section: Stress transfer, earthquake triggering, and time-dependent seismic hazard, *J. Geophys. Res.*, 110, B05S01, doi:10.1029/2005JB003692, 2005.

Stein, R. S., The role of stress transfer in earthquake occurrence, *Nature*, 402, 605–609, 1999.

Stein, R. S., A. A. Barka, and J. H. Dieterich, Progressive failure on the northern Anatolian fault since 1939 by earthquake stress triggering, *Geophys. J. Int.*, 128, 594–704, 1997.

Toda, S. and R. S. Stein, Toggling of seismicity by the 1997 Kagoshima earthquake couplet: A demonstration of time-dependent stress transfer, *J. Geophys. Res.*, 108(B12), 2567, doi: 10.1029/2003JB002527, 2003.

Toda, S., R. S. Stein, K. Richards-Dinger, and S. Bozkurt, Forecasting the evolution of seismicity in southern California: Animations built on earthquake stress transfer, *J. Geophys. Res.*, 110, B05S19, doi:10.1029/2004JB003389, 2005.

USGS, USGS Fast Moment Tensor Solution, Magnitude 6.7—Near the West Coast of Honshu, Japan, http://neic.usgs.gov/neis/eq_depot/2007/eq_070325_aiae/neic_aiae_q.html2007, 2007.

Yagi, Y., http://www.geo.tsukuba.ac.jp/press_HP/yagi/EQ/20070325/, 2007.

Yamanaka, Y., EIC Seismological Note: No. 185, 07/03/25 09:42(JCT) Near the west coast of Honshu, http://www.eri.u-tokyo.ac.jp/sanchu/Seismo_Note/2007/EIC185e.html, 2007.

S. Toda (e-mail: s-toda@aist.go.jp)